Observer based vector field guidance law for path following of underactuated surface vehicles in the presence of time-varying currents

Yinsong Qu

College of Intelligent Systems Science and Engineering
Harbin Engineering University
145 Nantong Street, Harbin, Heilongjiang, China

quyinsong@hrbeu.edu.cn

***Abstract* –In this paper, the path following control problem of underactuated surface vehicle in time-varying ocean currents is studied, and a novel observer based nonsingular vector field (ONVF) guidance law is developed. The motion states of surface vehicle are extended to three dimensions to avoid the singularity of the traditional vector field through the design of high-dimensional guidance law. In addition, the extended state observer is introduced to estimate the total kinematic uncertainty interference term caused by unknown time-varying currents and sway velocity. The proposed ONVF guidance law can effectively deal with unknown kinematic disturbances and provide real-time guidance signal. Furthermore, the neural-network base controller is developed to track the desired guidance signal accurately. The effectiveness of the guidance and control system is verified by comparative simulation experiments.**

Index Terms – path following, time-varying currents, extend state observer, nonsingular vector field, neural networks

I. INTRODUCTION

Path following of underactuated surface vehicles has attracted considerable attention for its excellent properties in civil and military uses [1]. Path following requires the surface vehicles to follow a given path without time constraints [2]. Therefore, guidance law design for path following is more flexible than trajectory tracking control.

There are many guidance methods for path following have been proposed, such as Line-of-sight (LOS) [3], vector filed (VF) [4], deep reinforcement learning (DRL) [5]. LOS is most often used in path following control, and there are also many improved LOS methods such as Integral LOS (ILOS) [6], sideslip observer based LOS [7], error constrained LOS (ELOS) [8]. However, these improved LOS methods either require that all states of robots be measured perfectly or the external flow be nonexistent or constant and irrotational, which is unrealistic in nautical navigation. Although DRL guidance law has a faster convergence than LOS, it requires prolonged offline training and has poor scalability. In [9], VF method is verified to be superior than LOS method in convergence speed and energy consumption. Unfortunately, compared with LOS, VF method is more often used in the guidance of ground robots [10][11] or unmanned aerial vehicles [12][13] instead of surface vehicles, it is difficult to apply VF method directly to underactuated surface vehicles due to the unknown sway velocity and currents. To solve this problem, we combine the nonsingular vector field (NVF) method proposed in [13] with extend state observer (ESO) technique to form a novel guidance law named as ONVF. The main contributions of this paper are list as follows.

1) The observer-based vector field guidance law is first proposed for path following of underactuated surface vehicles. The unknown sway velocity and time-varying currents are regarded as total kinematic disturbances, and the ONVF guidance law is designed to estimate and compensate for its adverse effects. Simulation experiments show that, compared with the NVF guidance law without observer, ONVF can produce more accurate guidance signal for path following in the presence of time-varying currents.

2) In this paper, an adaptive neural-network (NN) controller is designed to track the desired guidance signal accurately, which can effectively accommodate model uncertainties and unknown external disturbances. In addition, a dynamic auxiliary system is utilized to deal with the inputs saturation. Theoretical analysis and simulation experiments show that all the tracking errors can converge into a small domain of zero.

The remainder of this paper is organized as follows. Section II presents the surface vehicle model and control objective. The main result is given in Section III. The comparison simulations are conducted in Section IV. Section V concludes this paper.

II. PROBLEM FORMULATION

A. Surface vehicle model

The mathematical model of surface vehicle with double thrusters is given in [14]. Different from this model, we introduce a new state θ and the corresponding control input τ_θ to facilitate subsequent design of ONVF. The surface vehicle model with extended stated is given as follows.

$$\dot{\boldsymbol{\eta}} = u\boldsymbol{n}_1 + v\boldsymbol{n}_2 + \boldsymbol{v}_c \tag{1}$$

$$\dot{\boldsymbol{w}} = \boldsymbol{F}(u,v,r) + \boldsymbol{B}\boldsymbol{T} \tag{2}$$

$$\dot{\theta} = \tau_\theta \tag{3}$$

$$\dot{\psi} = r \tag{4}$$

$$\dot{v} = f_v - d_{33}v / m_{33} \tag{5}$$

where $\boldsymbol{\eta} = [x, y]^{\mathrm{T}}$ is the position vector composed by north

position x and east position y, $\boldsymbol{n}_1=[\cos(\psi),\sin(\psi)]^{\mathrm{T}}$ is the orientation vector, $\boldsymbol{n}_2=[-\sin(\psi),\cos(\psi)]^{\mathrm{T}}$ is perpendicular to $\boldsymbol{n}_1$, ψ denotes the heading angle, $\boldsymbol{v}_c=[v_{cx},v_{cy}]^{\mathrm{T}}$ represents the unknown time-variant current speed vector, $\boldsymbol{w}=[u,r]^{\mathrm{T}}$ is the velocity vector composed by surge velocity u and angular velocity r, v is sway velocity which is unknown, $\boldsymbol{F}(u,v,r)=[f_u,f_r]^{\mathrm{T}}$ is unknown kinetic disturbance vector, f_u, f_v and f_r are given as:

$$\begin{cases} f_u=(m_{22}vr-d_{11}u+\delta_u)/m_{11} \\ f_v=(-m_{11}ur+\delta_v)/m_{22} \\ f_r=((m_{11}-m_{22})uv-d_{33}r+\delta_r)/m_{33} \end{cases}$$

where $m_{ii},i=1,2,3$ are inertial masses, $d_{ii},i=1,2,3$ are linear damping terms, $\delta_i,i=u,v,r$ are external disturbances. $\boldsymbol{T}=[T_1,T_2]^{\mathrm{T}}$ is the control inputs vector composed by the thrust T_1 and T_2 produced by double thrusters. The matrix $\boldsymbol{B}$ is given by:

$$\boldsymbol{B}=\begin{bmatrix} 1/m_{11} & 1/m_{11} \\ d_p/m_{33} & -d_p/m_{33} \end{bmatrix} \tag{6}$$

where d_p is the is the lateral distance from the centerline of the surface vehicle to the centerline of each thruster. All the states and variables discussed above are shown in Fig. 1.

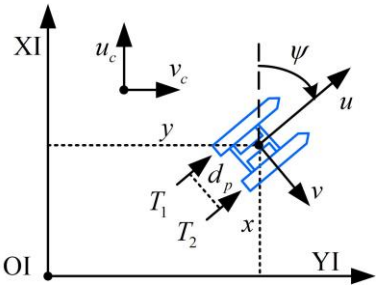

Fig. 1 coordinate system and states of surface vehicle

B. Real path and virtual path

The desired path (real path) can be parameterized by:

$$\mathcal{P}_{2\mathrm{D}}=\{\boldsymbol{\eta}_p\in\mathbb{R}^2: x_p=f_1(\theta),\ y_p=f_2(\theta),\theta\in\mathbb{R}\} \tag{7}$$

where $\boldsymbol{\eta}_p=[x_p,y_p]^{\mathrm{T}}$. To obtain the NVF guidance law, we need to extend the real path from two-dimensional (2D) space to three-dimensional (3D) space. The extended path is also called virtual path, which is described as follows.

$$\mathcal{P}_{3\mathrm{D}}=\{\bar{\boldsymbol{\eta}}_p\in\mathbb{R}^3: \phi_{p1}(\bar{\boldsymbol{\eta}}_p)=0,\ \phi_{p2}(\bar{\boldsymbol{\eta}}_p)=0\} \tag{8}$$

where $\bar{\boldsymbol{\eta}}_p=[\boldsymbol{\eta}_p^{\mathrm{T}},\theta]^{\mathrm{T}}$, $\phi_{p1}=x_p-f_1(\theta)$, $\phi_{p2}=y_p-f_2(\theta)$. To project the virtual path to the 2D space, the following project operator is introduced.

$$P^{prj}(\boldsymbol{\xi})=(\mathbf{I}_3-\hat{\boldsymbol{a}}\hat{\boldsymbol{a}}^{\mathrm{T}})\boldsymbol{\xi} \tag{9}$$

where $\boldsymbol{\xi}\in\mathbb{R}^3$, $\hat{\boldsymbol{a}}=[0,0,1]^{\mathrm{T}}$, $\mathbf{I}_3=\mathrm{diag}\{1,1,1\}$. The project operator will project the vector $\boldsymbol{\xi}\in\mathbb{R}^3$ onto the plane which is perpendicular to the vector $\hat{\boldsymbol{a}}$.

C. Control objective

The position states with the extended state of surface vehicle is denoted by $\bar{\boldsymbol{\eta}}=[\boldsymbol{\eta}^{\mathrm{T}},\theta]^{\mathrm{T}}$, then, the path following errors can be expressed by:

$$\phi_1=L_1(x-f_1(\theta)),\ \phi_2=L_2(y-f_2(\theta)) \tag{10}$$

where $0<L_1,L_2<1$ are constants. When $\phi_1=0,\phi_2=0$, there is $\bar{\boldsymbol{\eta}}\in\mathcal{P}_{3\mathrm{D}}$. Utilizing the project operator in (10), we can get that $\boldsymbol{\eta}=P^{prj}(\bar{\boldsymbol{\eta}})$, then we can further get $\boldsymbol{\eta}\in\mathcal{P}_{2\mathrm{D}}$. Based on the above analysis, control objective can be concluded as follows.

Control objective: In kinematics, under the assumption of the sufficiently fast and accurate tracking performance provided by NN controller, the proposed ONVF guidance law can guarantee that ϕ_1,ϕ_2 satisfy that $\lim_{t\to\infty}\|\phi_1,\phi_2\|<d_1$ in the presence of time-varying currents for a sufficiently small constant $d_1>0$. In kinetics, the developed NN controller can guarantee that the surge and yaw velocity u,r can track the desired guidance signal u_c,r_c rapidly and accurately under the inputs saturation and unknown environmental disturbances, i.e., $\lim_{t\to\infty}\|\tilde{u},\tilde{r}\|<d_2$, where $\tilde{u}=u-u_c$, $\tilde{r}=r-r_c$, and $d_2>0$ is a sufficiently small constant. Furthermore, all the closed-loop errors are bounded.

III. Main Result

A. ONVF guidance law design

Let $\boldsymbol{n}_3=v\boldsymbol{n}_2+\boldsymbol{v}_c$ be the total kinematic disturbance. Define the estimation errors as $\tilde{\boldsymbol{\eta}}=\boldsymbol{\eta}-\breve{\boldsymbol{\eta}}$, $\tilde{\boldsymbol{n}}_3=\boldsymbol{n}_3-\breve{\boldsymbol{n}}_3$. The kinematic disturbance observer is designed as follows.

$$\dot{\breve{\boldsymbol{\eta}}}=u\boldsymbol{n}_1+\breve{\boldsymbol{n}}_3+\boldsymbol{K}_{o1}\tilde{\boldsymbol{\eta}} \tag{11}$$

$$\dot{\breve{\boldsymbol{n}}}_3=\boldsymbol{K}_{o2}\tilde{\boldsymbol{\eta}} \tag{12}$$

Combining (1), errors dynamics can be obtained as:

$$\dot{\tilde{\boldsymbol{\eta}}}=-\boldsymbol{K}_{o1}\tilde{\boldsymbol{\eta}}+\tilde{\boldsymbol{n}}_3 \tag{13}$$

$$\dot{\tilde{\boldsymbol{n}}}_3=-\boldsymbol{K}_{o2}\tilde{\boldsymbol{\eta}}+\dot{\boldsymbol{n}}_3 \tag{14}$$

Due to the bounded value of $\dot{v},\dot{\boldsymbol{n}}_2$ and $\dot{\boldsymbol{v}}_c$, the derivative of $\boldsymbol{n}_3$ is also bounded. Then, we can get the estimation error $\tilde{\boldsymbol{\eta}}$ and $\tilde{\boldsymbol{n}}_3$ are uniformly stable according to [15](Corollary 2).

Let $\tilde{u}=u-u_c$. We can rewrite (1) as:

$$\dot{\boldsymbol{\eta}} = u_d \boldsymbol{n}_1 + \breve{\boldsymbol{n}}_3 + \tilde{\boldsymbol{n}}_3 + \tilde{u}\boldsymbol{n}_1 \tag{15}$$

Let $\boldsymbol{n}_4 = u_d \boldsymbol{n}_1 + \breve{\boldsymbol{n}}_3$, $\tilde{\boldsymbol{n}}_4 = \tilde{\boldsymbol{n}}_3 + \tilde{u}\boldsymbol{n}_1$, $\boldsymbol{n}_5 = [\boldsymbol{n}_4^{\mathrm{T}}, \tau_\theta]^{\mathrm{T}}$, $\tilde{\boldsymbol{n}}_5 = [\tilde{\boldsymbol{n}}_4, 0]^{\mathrm{T}}$. Then, we can rewrite (15) and (3) as the compact form as following.

$$\dot{\tilde{\boldsymbol{\eta}}} = \|\boldsymbol{n}_4\| \hat{\boldsymbol{n}}_5' + \tilde{\boldsymbol{n}}_5 \tag{16}$$

where $\hat{\boldsymbol{n}}_5' = \boldsymbol{n}_5 / \|\boldsymbol{n}_4\|$. The expression (16) will used in proof of Theorem 1. The desired 3D vector field $\boldsymbol{n}_d$ is given as:

$$\boldsymbol{n}_d = \boldsymbol{n}_{dX} - \boldsymbol{N}\boldsymbol{K}_n \boldsymbol{e}_\phi \tag{17}$$

where $\boldsymbol{N} = [\nabla\phi_{p1}, \nabla\phi_{p2}]$, $\boldsymbol{n}_{dX} = \nabla\phi_{p1} \times \nabla\phi_{p2}$. According to (10), $\boldsymbol{n}_d$ can be calculated by:

$$\boldsymbol{n}_d = \begin{bmatrix} L_1 L_2 f_1'(\theta) - L_1\phi_1 \\ L_1 L_2 f_2'(\theta) - L_2\phi_2 \\ L_1 L_2 - L_1\phi_1 f_1'(\theta) - L_2\phi_2 f_2'(\theta) \end{bmatrix}$$

Let $\boldsymbol{n}_{pd} = [n_{d(1)}, n_{d(2)}]^{\mathrm{T}}$, where $\boldsymbol{n}_{d(1)}$ and $\boldsymbol{n}_{d(2)}$ represent the first two elements of $\boldsymbol{n}_d$. Let $\hat{\boldsymbol{n}}_d' = \boldsymbol{n}_d / \|\boldsymbol{n}_{pd}\|$. According to the properties of $\hat{\boldsymbol{n}}_d'$, when $\hat{\boldsymbol{n}}_5' = \hat{\boldsymbol{n}}_d'$ and $\tilde{\boldsymbol{n}}_5$ is bounded, the integral curve defined in (16) will converge into small domain of $\mathcal{P}_{3\mathrm{D}}$. Therefore, we need to design a guidance law to make $\hat{\boldsymbol{n}}_5'$ satisfy that $\lim_{t\to\infty} \|\hat{\boldsymbol{n}}_5' - \hat{\boldsymbol{n}}_d'\| < d_3$, where $d_3 > 0$ is a sufficiently small constant. The desired guidance law is given in the following theorem.

Theorem 1. Considering the kinematics (16) and (4), and the desired 3D vector field (17), the desired guidance law r_c is designed as follows.

$$r_c' = \dot{\chi}_d - k_r \hat{\boldsymbol{n}}_4^{\mathrm{T}} \boldsymbol{E} \hat{\boldsymbol{n}}_{pd} \tag{18}$$

$$r_c = \frac{\|\boldsymbol{n}_4\| r_c' + \hat{\boldsymbol{n}}_4^{\mathrm{T}} \boldsymbol{E} \dot{\breve{\boldsymbol{n}}}_3}{u_d \hat{\boldsymbol{n}}_4^{\mathrm{T}} \boldsymbol{n}_1} \tag{19}$$

$$\tau_\theta = \|\boldsymbol{n}_4\| \hat{\boldsymbol{n}}_{d(3)}' \tag{20}$$

$$\dot{\chi}_d = -\hat{\boldsymbol{n}}_{pd}^{\mathrm{T}} \boldsymbol{E} \boldsymbol{J}(\boldsymbol{n}_{pd}) \dot{\tilde{\boldsymbol{\eta}}} / \|\boldsymbol{n}_{pd}\| \tag{21}$$

where $\boldsymbol{J}(\boldsymbol{n}_{pd})$ is the Jacobian matrix of $\boldsymbol{n}_{pd}$, which is calculated by:

$$\boldsymbol{J}(\boldsymbol{n}_{pd}) = \begin{bmatrix} -L_1 & 0 & L_1 L_2 f_1'(\theta) + L_1 f_1'(\theta) \\ 0 & -L2 & L_1 L_2 f_2'(\theta) + L_2 f_2'(\theta) \end{bmatrix}$$

Under the assumption that $\tilde{r} = r - r_c$ is sufficiently small, then, the guidance law can guarantee that the integral curve defined in (16) will converge into small domain of $\mathcal{P}_{3\mathrm{D}}$. Furthermore, the integral curve defined in (1) will converge into small domain of $\mathcal{P}_{2\mathrm{D}}$.

Proof: Define the orientation error as $\boldsymbol{e}_{ori} = \hat{\boldsymbol{n}}_5' - \hat{\boldsymbol{n}}_d'$. In the following, the proof will be divided into two parts. In the first step, we prove the stability of $\boldsymbol{e}_{ori}$ guaranteed by the desired guidance law r_c. Let $r = r_c + \tilde{r}$. According to virtual control law (20), we can get $e_{ori(3)} = 0$. Therefore, we only need consider $\boldsymbol{e}_{ori}' = [\boldsymbol{e}_{ori(1)}, \boldsymbol{e}_{ori(2)}]$, i.e., $\boldsymbol{e}_{ori}' = \hat{\boldsymbol{n}}_4 - \hat{\boldsymbol{n}}_{pd}$. The derivatives of $\hat{\boldsymbol{n}}_4, \hat{\boldsymbol{n}}_{pd}$ can be obtained as:

$$\dot{\hat{\boldsymbol{n}}}_4 = (r' + \tilde{r}')\boldsymbol{E}\hat{\boldsymbol{n}}_4, \quad \dot{\hat{\boldsymbol{n}}}_4 = \dot{\chi}_d \boldsymbol{E}\hat{\boldsymbol{n}}_4 \tag{22}$$

where $r' = -\hat{\boldsymbol{n}}_4^{\mathrm{T}} \boldsymbol{E}(u_d r_c \boldsymbol{E}\boldsymbol{n}_1 + \dot{\breve{\boldsymbol{n}}}_3) / \|\boldsymbol{n}_4\|$, $\tilde{r}' = u_d \tilde{r} \hat{\boldsymbol{n}}_4^{\mathrm{T}} \boldsymbol{n}_1 / \|\boldsymbol{n}_4\|$, χ_d is the orientation angle of $\hat{\boldsymbol{n}}_4$. Considering Lyapunov candidate $V_1 = 0.5 \boldsymbol{e}_{ori}'^{\mathrm{T}} \boldsymbol{e}_{ori}'$, we take its derivative as:

$$\begin{aligned} \dot{V}_1 &= (\hat{\boldsymbol{n}}_4 - \hat{\boldsymbol{n}}_{pd})^{\mathrm{T}} (\dot{\hat{\boldsymbol{n}}}_4 - \dot{\hat{\boldsymbol{n}}}_{pd}) \\ &= (r' - \dot{\chi}_d + \tilde{r}') \hat{\boldsymbol{n}}_4^{\mathrm{T}} \boldsymbol{E} \boldsymbol{n}_{pd} \\ &= -k_r (\hat{\boldsymbol{n}}_4^{\mathrm{T}} \boldsymbol{E} \boldsymbol{n}_{pd})^2 + \tilde{r}' \hat{\boldsymbol{n}}_4^{\mathrm{T}} \boldsymbol{E} \boldsymbol{n}_{pd} \\ &\le -(k_r - \frac{1}{2\varepsilon_1})(\hat{\boldsymbol{n}}_4^{\mathrm{T}} \boldsymbol{E} \boldsymbol{n}_{pd})^2 + \gamma_1 \end{aligned}$$

where $\gamma_1 = \frac{\varepsilon_1}{2}\|\tilde{r}'\|^2$ is bounded. According to the Lyapunov stability theory, $\boldsymbol{e}_{ori}'$ is uniformly bounded. In the second step, we prove the integral curve defined in (1) will converge into small domain of $\mathcal{P}_{2\mathrm{D}}$ guaranteed by the sufficiently small error $\boldsymbol{e}_{ori}'$ proved in the first step. Let $\hat{\boldsymbol{n}}_5 = \hat{\boldsymbol{n}}_d + \boldsymbol{e}_{ori}$. Considering the Lyapunov candidate as $V_1 = 0.5 \boldsymbol{e}_\phi^{\mathrm{T}} \boldsymbol{K}_n \boldsymbol{e}_\phi$, we take its derivative as:

$$\begin{aligned} \dot{V}_2 &= \boldsymbol{e}_\phi^{\mathrm{T}} \boldsymbol{K}_n \boldsymbol{N}^{\mathrm{T}} \dot{\tilde{\boldsymbol{\eta}}} \\ &= \boldsymbol{e}_\phi^{\mathrm{T}} \boldsymbol{K}_n \boldsymbol{N}^{\mathrm{T}} (\|\boldsymbol{n}_4\| \hat{\boldsymbol{n}}_d' + \|\boldsymbol{n}_4\| \boldsymbol{e}_{ori} + \tilde{\boldsymbol{n}}_5) \\ &= -\frac{\|\boldsymbol{n}_4\|}{\|\boldsymbol{n}_{pd}\|} \boldsymbol{e}_\phi^{\mathrm{T}} \boldsymbol{K}_n \boldsymbol{N}^{\mathrm{T}} \boldsymbol{N} \boldsymbol{K}_n \boldsymbol{e}_\phi + \boldsymbol{e}_\phi^{\mathrm{T}} \boldsymbol{K}_n \boldsymbol{N}^{\mathrm{T}} (\|\boldsymbol{n}_4\| \boldsymbol{e}_{ori}'' + \tilde{\boldsymbol{n}}_5) \\ &\le -\kappa_0 \|\boldsymbol{e}_\phi\|^2 + \gamma_2 \end{aligned}$$

where $\gamma_2 = \frac{\varepsilon_2}{2}\|\boldsymbol{n}_4\|^2 \|\boldsymbol{e}_{ori}''\|^2 + \frac{\varepsilon_2}{2}\|\tilde{\boldsymbol{n}}_5\|^2$ is bounded, $\kappa_0 = (\frac{\|\boldsymbol{n}_4\|}{\|\boldsymbol{n}_{pd}\|} - \frac{1}{\varepsilon_2})\mu_0 > 0$, where μ_0 is the smallest eigenvalue of $\boldsymbol{K}_n \boldsymbol{N}^{\mathrm{T}} \boldsymbol{N} \boldsymbol{K}_n$. According Lyapunov stability theory, we can conclude that is uniformly bounded.

B. Adaptive neural-network controller

Considering the inputs saturation, we can rewrite (2) as:

$$\dot{\boldsymbol{w}} = \boldsymbol{F}(u, v, r) + \boldsymbol{B}\boldsymbol{T}_c - \boldsymbol{B}\boldsymbol{\Delta}_T \tag{23}$$

where $\boldsymbol{T}_c = [T_{c1}, T_{c2}]^{\mathrm{T}}$ is saturated version of $\boldsymbol{T}$ defined as:

$$T_{ci} = \mathrm{Sat}(T_i) = \begin{cases} T_{max} & , \quad T_i \geq T_{max} \\ T_i & , \quad T_{min} < T_i < T_{max} \\ T_{min} & , \quad T_i \leq T_{min} \end{cases} \tag{24}$$

where $i = 1, 2$, $\mathrm{Sat}(\bullet)$ is saturation function. Then, the auxiliary system can be designed as:

$$\dot{\boldsymbol{\lambda}} = -\boldsymbol{A}\boldsymbol{\lambda} - \boldsymbol{B}\boldsymbol{\Delta}_T \tag{25}$$

Define tracking error $\boldsymbol{e}_w = \boldsymbol{w} - \boldsymbol{w}_d - \boldsymbol{\lambda}$. The derivative of e_w is calculated by:

$$\dot{\boldsymbol{e}}_w = \boldsymbol{F}(u, v, r) + \boldsymbol{B}\boldsymbol{T}_c - \dot{\boldsymbol{w}}_d + \boldsymbol{A}\boldsymbol{\lambda} \tag{26}$$

Since the nonlinear term $\boldsymbol{F}(u, v, r)$ is unknown, we need to approximate it by neural networks as follows.

$$\boldsymbol{F}(u, v, r) = \boldsymbol{W}^T \boldsymbol{\Phi}(\boldsymbol{X}) + \boldsymbol{\zeta}(\boldsymbol{X}) \tag{27}$$

where $\boldsymbol{W}$ is the desired weight matrix, which is unknown, $\boldsymbol{X}$ is the inputs vector of NN, $\boldsymbol{\Phi}(\boldsymbol{X})$ is radial basis function, $\boldsymbol{\zeta}(\boldsymbol{X})$ is the approximate error [16]. Then, we can get the proportional (P) type feedback control law as:

$$\boldsymbol{T}_c = \boldsymbol{B}^{-1}(\dot{\boldsymbol{w}}_d - \boldsymbol{A}\boldsymbol{\lambda} - \hat{\boldsymbol{W}}^T \boldsymbol{\Phi}(\boldsymbol{X}) - \boldsymbol{K}_w \boldsymbol{e}_w) \tag{28}$$

where $\hat{\boldsymbol{W}}$ is the estimate value of $\boldsymbol{W}$. Bring (28) and (27) into (26), we can get:

$$\dot{\boldsymbol{e}}_w = \tilde{\boldsymbol{W}}\boldsymbol{\Phi}(\boldsymbol{X}) - \boldsymbol{K}_w \boldsymbol{e}_w + \boldsymbol{\zeta}(\boldsymbol{X}) \tag{29}$$

The update law of $\hat{\boldsymbol{W}}$ can be chosen as:

$$\dot{\hat{\boldsymbol{W}}} = \Gamma_W (\boldsymbol{\Phi}(\boldsymbol{X}) \boldsymbol{e}_w^T - \boldsymbol{k}_W \hat{\boldsymbol{W}}) \tag{30}$$

The ONVF guidance law and NN controller are completed here. The guidance and control system proposed in this paper is shown in Fig. 2.

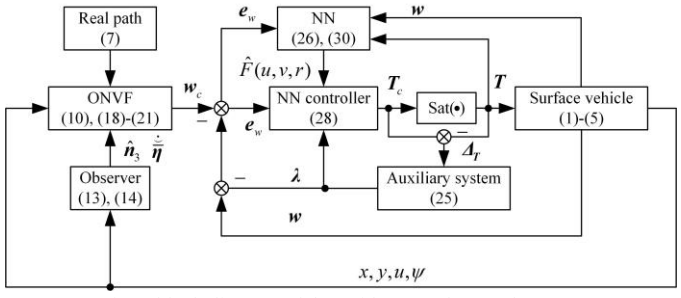

Fig. 2 block diagram of the guidance and control system

C. Main result

Theorem 2. Considering the surface vehicle model (23), with the auxiliary system (25), P feedback control law (28) and the update law (30), then, the error dynamic (29) is uniformly bounded. In addition, the path following errors ϕ_1, ϕ_2 will converge into a small domain of zero, and all the closed-loop errors are uniformly bounded.

Proof: Considering the Lyapunov candidate as $V_3 = 0.5\boldsymbol{e}_w^{\mathrm{T}}\boldsymbol{e}_w + 0.5\,\mathrm{tr}(\hat{\boldsymbol{W}}^{\mathrm{T}}\Gamma_W^{-1}\hat{\boldsymbol{W}}) + 0.5\boldsymbol{\lambda}^{\mathrm{T}}\boldsymbol{\lambda}$, we take its derivative as follows.

$$\begin{aligned} \dot{V}_3 &= -\boldsymbol{e}_w^{\mathrm{T}}\boldsymbol{K}_w\boldsymbol{e}_w + \mathrm{tr}(\tilde{\boldsymbol{W}}^{\mathrm{T}}(\boldsymbol{\Phi}(\boldsymbol{X})\boldsymbol{e}_w^{\mathrm{T}} - \Gamma_W^{-1}\dot{\hat{\boldsymbol{W}}}) - \boldsymbol{\lambda}^{\mathrm{T}}\boldsymbol{A}\boldsymbol{\lambda} + \\ &\quad \boldsymbol{e}_w^{\mathrm{T}}\boldsymbol{\zeta}(\boldsymbol{X}) - \boldsymbol{\lambda}^{\mathrm{T}}\boldsymbol{B}\boldsymbol{\Delta}_T \\ &\leq -(\mu_1 - \frac{1}{2\varepsilon_3})\boldsymbol{e}_w^{\mathrm{T}}\boldsymbol{e}_w - (\mu_2 - \frac{1}{2\varepsilon_3})\boldsymbol{\lambda}^{\mathrm{T}}\boldsymbol{\lambda} - k_W\mu_3\,\mathrm{tr}(\tilde{\boldsymbol{W}}^{\mathrm{T}}\Gamma_W^{-1}\tilde{\boldsymbol{W}}) + \\ &\quad k_W\,\mathrm{tr}(\tilde{\boldsymbol{W}}^{\mathrm{T}}\boldsymbol{W}) + \frac{\varepsilon_3}{2}\|\boldsymbol{\zeta}(\boldsymbol{X})\| + \frac{\varepsilon_3}{2}\|\boldsymbol{B}\boldsymbol{\Delta}_T\| \\ &\leq -\kappa_1\boldsymbol{e}_w^{\mathrm{T}}\boldsymbol{e}_w - \kappa_2\boldsymbol{\lambda}^{\mathrm{T}}\boldsymbol{\lambda} - \kappa_3\,\mathrm{tr}(\tilde{\boldsymbol{W}}^{\mathrm{T}}\Gamma_W^{-1}\tilde{\boldsymbol{W}}) + \gamma_3 \\ &\leq -\kappa V_3 + \gamma_3 \end{aligned}$$

where $\gamma_3 = \frac{\varepsilon_3}{2}\|\boldsymbol{\zeta}(\boldsymbol{X})\| + \frac{\varepsilon_3}{2}\|\boldsymbol{B}\boldsymbol{\Delta}_T\|$, $\kappa = \min\{\kappa_1, \kappa_2, \kappa_3\}$, $\kappa_1 = \mu_1 - \frac{1}{2\varepsilon_3}$, $\kappa_2 = \mu_2 - \frac{1}{2\varepsilon_3}$, $\mu_i, i = 1, 2, 3$ represent the smallest eigenvalue of $\boldsymbol{K}_w$, $\boldsymbol{A}$ and $\boldsymbol{\Gamma}_W$ respectively. The following inequalities are utilized during the above derivation.

$$\begin{cases} \mathrm{tr}(\tilde{\boldsymbol{W}}^{\mathrm{T}}\boldsymbol{W}) \leq \frac{1}{2}\|\tilde{\boldsymbol{W}}\|_F^2 + \frac{1}{2}\|\boldsymbol{W}\|_F^2 \\ \boldsymbol{\lambda}^{\mathrm{T}}\boldsymbol{B}\boldsymbol{\Delta}_T \leq \frac{1}{2}\|\boldsymbol{\lambda}\|^2 + \frac{1}{2}\|\boldsymbol{B}\boldsymbol{\Delta}_T\|^2 \\ \boldsymbol{e}_w^{\mathrm{T}}\boldsymbol{\zeta}(\boldsymbol{X}) \leq \frac{1}{2}\|\boldsymbol{e}_w\|^2 + \frac{1}{2}\|\boldsymbol{\zeta}(\boldsymbol{X})\|^2 \end{cases}$$

We can obtain that γ_3 is bounded reasonably. According Lyapunov stability theory, we can conclude that the all error dynamic (29) is uniformly bounded. And combining Theorem 1, we can further get the path following errors ϕ_1, ϕ_2 will converge into a small domain of zero and all the tracking errors are uniformly bounded.

IV. Simulations

This section presents simulation results on the proposed guidance and control strategy for path following. The USV model is given by [14], the parameters are as $m_{11} = 50.5\mathrm{kg}$, $m_{22} = 84.36\mathrm{kg}$, $m_{33} = 17.21\mathrm{kg}$, $d_{11} = 151.57\mathrm{kg/s}$, $d_{22} = 132.5\mathrm{kg/s}$, $d_{33} = 34.56\mathrm{kg/s}$, $d_p = 0.26\mathrm{kgm}$. The initial value of states are given as $\boldsymbol{\eta}_0 = [10, 10]^{\mathrm{T}}$, $w_0 = [0, 0]^{\mathrm{T}}$, $\theta_0 = 0$, $v_0 = 0$ and $\psi_0 = 0$. We parameterize the real path as:

$$\begin{cases} x_p = \theta \\ y_p = 20\sin(\pi\theta / 25) \end{cases} \tag{31}$$

The time-varying current is chosen as:

$$\begin{cases} \boldsymbol{v}_c = [0,0]^{\mathrm{T}} & ,t \le 50 \\ \boldsymbol{v}_c = [4\sin(0.12t), 4\cos(0.12t)]^{\mathrm{T}} & ,t > 50 \end{cases} \tag{32}$$

The kinetic disturbances are chosen as:

$$\begin{cases} \delta_u = 15\sin(0.3t)\cos(0.2t) + 15 \\ \delta_v = 15\sin(0.3t)\cos(0.2t) + 10 \\ \delta_r = 10\sin(0.3t)\cos(0.2t) + 10 \end{cases} \tag{33}$$

The parameters for guidance law and control law are shown in Table I, where $\mathrm{diag}\{\mathrm{ones}\{9,1\}\}$ represents 9th order unit diagonal matrix, n_{in}, n_{hid} and n_{out} represent number of inputs, hidden neurons and outputs of neural networks.

Table I
parameters for ONVF guidance law and NN controller

ONVF	NN controller
$\boldsymbol{K}_{o1} = \mathrm{diag}\{8,8\}$	$\boldsymbol{K}_w = \mathrm{diag}\{4,2\}$
$\boldsymbol{K}_{o2} = \mathrm{diag}\{10,10\}$	$\boldsymbol{A} = \mathrm{diag}\{1,0.5\}$
$\boldsymbol{K}_n = \mathrm{diag}\{0.6,0.6\}$	$n_{in} = 4$, $n_{hid} = 9$, $n_{out} = 2$
$l_n = 1$, $k_r = 5$	$\boldsymbol{\Gamma}_W = 2.5\mathrm{diag}\{\mathrm{ones}\{9,1\}\}$
$L_1 = 0.001$, $L_2 = 0.001$	$k_W = 0.005$, $\boldsymbol{X} = [u, r, ur, (\boldsymbol{BT})^{\mathrm{T}}]^{\mathrm{T}}$

To verify the effectiveness and robustness of ONVF, we conduct a comparative experiment on the two methods, ONVF and NVF. The simulation results are shown in Fig. 3-Fig. 8. As shown in Fig. 3 and the last subgraph of Fig. 4, ONVF can provide higher tracking accuracy than NVF under the time-varying currents. Since there is no time-varying current for $t \le 50$s, both methods can track the predetermined path accurately, the obvious difference occurs when $t > 50$s, ONVF has higher tracking accuracy than NVF due to the time-varying current. It can be seen from Fig. 4 that all tracking errors of the closed-loop system converge into the small region of zero.

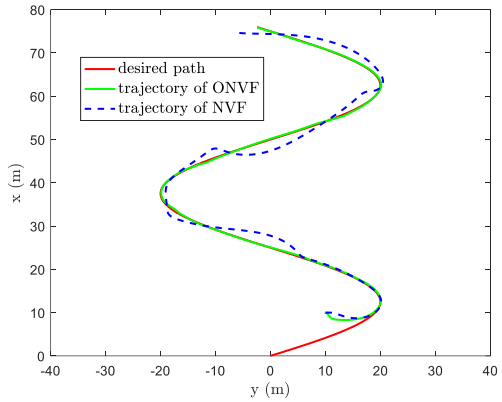

Fig. 3 real path and trajectories of ONVF and NVF

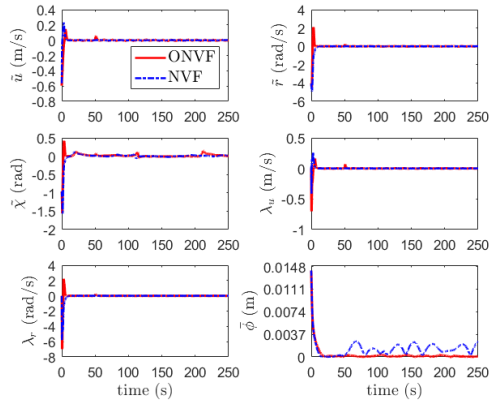

Fig. 4 tracking errors of ONVF and NVF

Fig. 5 shows the role of virtual state θ, that is, extending the real path from 2D to 3D. As shown in Fig. 5, the virtual trajectory can converge to the virtual path, simultaneously, the real trajectory of surface vehicle converges to the real path.

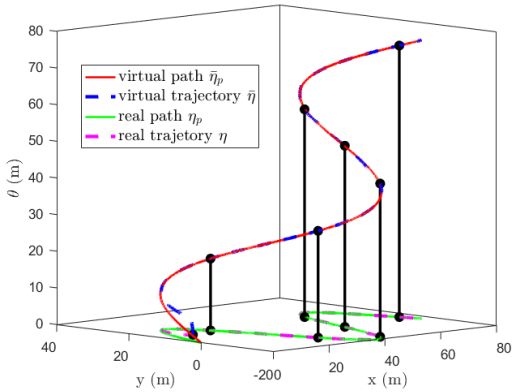

Fig. 5 real path and virtual path of ONVF

As shown in Fig. 6 and Fig. 7, the extended state observer and the neural networks can accurately estimate the kinematic disturbances and kinetic disturbances respectively.

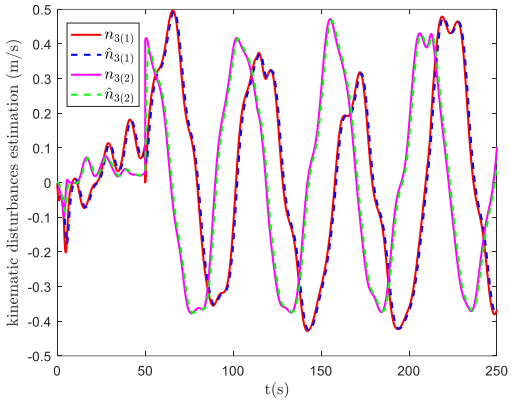

Fig. 6 kinematic disturbances estimation of ONVF

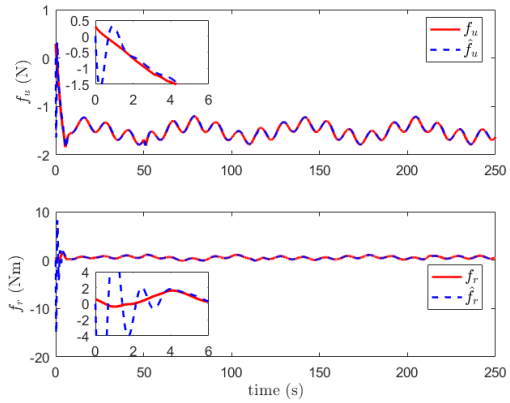

Fig. 7 kinetic disturbances estimation of ONVF

As shown in Fig. 8, although the control commands exceed the thrust limits of the thrusters, the actual outputs of the thrusters do not exceed the thrust limit due to the existence of the auxiliary dynamic system. It verifies that auxiliary system can handle the inputs saturation perfectly.

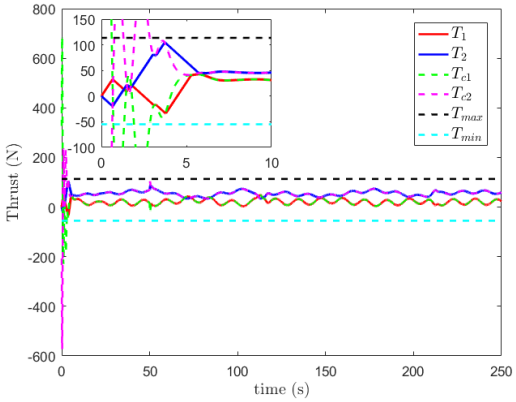

Fig. 8 control command $\boldsymbol{T}_c$ and constrained input $\boldsymbol{T}$ of ONVF

V. Conclusion

A new ONVF guidance law for path following control of underactuated surface vehicles was developed. The proposed guidance law can provide accurate guidance signal in the time-varying currents. In addition, the NN controller can track the guidance signal perfectly even under the external disturbances. All the closed-loop errors are proved uniformly bounded by Lyapunov stability theory. Finally, the comparative simulations are conducted to verify the effectiveness and robustness of the proposed guidance and control system.

References

[1] Deng, Y., Zhang, X., Im, N., Zhang, G., & Zhang, Q. Model-Based Event-Triggered Tracking Control of Underactuated Surface Vessels With Minimum Learning Parameters. IEEE Transactions on Neural Networks and Learning Systems, 2019, pp. 1–14,.

[2] Yao, W., & Cao, M. Path following control in 3D using a vector field. Automatica, 117, 108957, 2020.

[3] Fossen, T. I., Breivik, M., & Skjetne, R. Line-of-sight path following of underactuated marine craft. IFAC Proceedings Volumes, 36(21), 2003, pp. 211-216.

[4] Xu, H. T., Fossen T. and Guedes Soares C. Uniformly semiglobally exponential stability of vector field guidance law and autopilot for path-following, European Journal of Control, 53, 2020, pp. 88-97.

[5] Gonzalez-Garcia, A., Castaneda, H., & Garrido, L. USV Path-Following Control Based On Deep Reinforcement Learning and Adaptive Control. Global Oceans 2020: Singapore – U.S. Gulf Coast, 2020.

[6] Caharija, W., Pettersen, K. Y., Bibuli, M., Calado, P., Zereik, E., Braga, J., … Bruzzone, G. Integral Line-of-Sight Guidance and Control of Underactuated Marine Vehicles: Theory, Simulations, and Experiments. IEEE Transactions on Control Systems Technology, 24(5), 2016, pp. 1623–1642.

[7] Xia, G., Wang, X., Zhao, B., Han, Z., & Yang, Y. LOS Guidance Law for Path Following of USV based on Sideslip Observer. 2019 Chinese Automation Congress (CAC), 2019.

[8] Zheng, Z., Sun, L., & Xie, L. Error-Constrained LOS Path Following of a Surface Vessel With Actuator Saturation and Faults. IEEE Transactions on Systems, Man, and Cybernetics: Systems, 1–12, 2017.

[9] P. B. Sujit, S. Saripalli and J. B. Sousa, "Unmanned Aerial Vehicle Path Following: A Survey and Analysis of Algorithms for Fixed-Wing Unmanned Aerial Vehicless," in IEEE Control Systems Magazine, vol. 34, no. 1, Feb. 2014, pp. 42-59.

[10] Michałek, M. M., & Gawron, T. VFO Path following Control with Guarantees of Positionally Constrained Transients for Unicycle-Like Robots with Constrained Control Input. Journal of Intelligent & Robotic Systems, 89(1-2), 2017, pp. 191-210.

[11] Kapitanyuk, Y. A., Proskurnikov, A. V., & Cao, M. A Guiding Vector-Field Algorithm for Path-Following Control of Nonholonomic Mobile Robots. IEEE Transactions on Control Systems Technology, 26(4), 2018, pp. 1371-1385.

[12] Wilhelm, J. P., & Clem, G. Vector Field UAV Guidance for Path Following and Obstacle Avoidance with Minimal Deviation. Journal of Guidance, Control, and Dynamics, 2019, pp. 1-9.

[13] Yao, W., de Marina, H. G., Lin, B., & Cao, M. Singularity-Free Guiding Vector Field for Robot Navigation. IEEE Transactions on Robotics, 37(4), 2021, pp. 1206-1221.

[14] Li, C., Jiang, J., Duan, F., Liu, W., Wang, X., Bu, L., Yang, G. Modeling and Experimental Testing of an Unmanned Surface Vehicle with Rudderless Double Thrusters. Sensors, 19(9), 2051, 2019.

[15] Guo, B.-Z., & Zhao, Z. On the convergence of an extended state observer for nonlinear systems with uncertainty. Systems & Control Letters, 60(6), 2011, pp. 420-430.

[16] Xia, G., Wang, X., Zhao, B., Han, Z., & Zheng, L Adaptive Neural Path Following Control of Underactuated Surface Vessels with Input Saturation. IEEE Access, 2020